Published in final edited form as:
Chem Mater. 2007 ; 19(16): 3902–3911. doi:10.1021/cm070238n.

Preparation and Characterization of Porous Gold and its Application as a Platform for Immobilization of Acetylcholine Esterase

Olga V. Shulga[1,2], **Kenise Jefferson**[1,2], **Abdul R. Khan**[1], **Valerian T. D'Souza**[1], **Jingyue Liu**[1,2], **Alexei V. Demchenko**[1,2], and **Keith J. Stine**[1,2*]

1*Department of Chemistry and Biochemistry, University of Missouri - St. Louis, St. Louis, Missouri, 63121*

2*Center of Molecular Electronics, University of Missouri - St. Louis, St. Louis, Missouri, 63121*

Abstract

We report a method for fabrication of free-standing porous gold material with high surface area, and well-defined, tunable pore morphology. Porous gold is formed via a simple procedure which involves an acidic treatment of a commercially available complex white-gold alloy. We used SEM and AFM techniques to characterize the surface morphology, size and shape of the meso-pores as well as the surface roughness of the prepared porous gold samples. Formation of self-assembled monolayers of a flavin sulfide on the gold surface was used to estimate the total surface area of porous gold material. The monolayers were found to be electrochemically active by cyclic and square-wave voltammetry. It was found that 24 hour HNO_3 treatment gave a 12,400 times surface enlargement and resulted in a surface area of 14.2 m^2/g, whereas 72 hour HNO_3 treatment resulted in a 6900 times surface enlargement and a surface area of 8.7 m^2/g. In addition, the enzyme acetylcholine esterase was immobilized on the different porous gold surfaces in order to demonstrate biocompatibility of the porous gold material. Kinetic parameters and the amount of the immobilized acetylcholine esterase were determined.

Introduction

Porous gold has attracted considerable attention in a wide range of applications including catalysis, fuel cells, [1, 2] cell imaging,[3] energy storage,[4] investigation of the critical behavior of liquid helium[5] and the development of chemical sensors[6–8] due to its high surface-to-volume ratio, stability and biocompatibility.

Common methods for preparation of porous gold include formation of a gold/silver alloy used as a precursor followed by de-alloying with concentrated nitric acid during which silver is removed, resulting in a highly porous structure of gold. [9] Dealloying is frequently followed by thermal annealing in order to adjust the pore size. Gold/silver alloys can be prepared by electrodeposition from $Au(CN)_2^-$ and $Ag(CN)_2^-$ solution at −1.2V[10], by arc melting of pure elements in an ampoule under inert atmosphere[11, 12] or by sputtering of pure gold and silver onto a substrate. [13] Other methods of porous gold preparation include the use of templates, [14] thermal decomposition of Au_2O_3, sublimation of iodine from Au-I_2 pressed powders,[15] electrochemical treatment of polycrystalline gold[16] and dissolution of gold chloride in a dextran solution followed by heating to 600–800°C.[17] Porous gold can also be generated by

*Corresponding Author, Keith J. Stine, Department of Chemistry and Biochemistry, University of Missouri - St. Louis, St. Louis, Missouri, 63121, Phone: (314) 516-5346, Fax: (314) 516-5342, e-mail: kstine@umsl.edu.

applying a sufficiently positive electrochemical potential to Au-containing alloy films,[18,19] and by electrochemically dealloying Au-Zn films prepared on Au wires. [20]

One of the most attractive avenues for the application of porous gold material is its use as a solid support for immobilization of biomolecules such as enzymes and antibodies. Immobilization of enzymes on solid supports plays a major role in modern biosensor technology, while immobilized antibodies are often used to devise highly selective immunoassays for diagnostic purposes. Duan and Meyerhoff[21, 22] used gold coated porous nylon membranes to develop a colorimetric ELISA for human chorionic gonadatropin (hCG). Ducey and Meyerhoff [23] used microporous gold as an electrochemical biosensor for flow injection HPLC analysis and postcolumn detection of catechol and phenol. Jurica [24] and co-workers used porous gold electrodes prepared by potentiostatic or galvanostatic treatment of disposable porous working electrodes with solutions of $HAuCl_4$, for flow-through stripping coulometric detection of As(III) and total As in water samples. Noort and co-workers[8] demonstrated the application of porous gold for immobilization of human anti-myoglobin. A porous gold nanoparticle – $CaCO_3$ hybrid material was used by Cai and co-workers for immobilization of horseradish peroxidase. [25] Thin films of porous gold of 20–100 nm thickness have been prepared on the surface of microcantilevers, and then modified with a thiolated β-cyclodextrin derivative and shown to sensitively detect tetrachloroethylene vapor. [26] The modified cantilevers were also applied to detect biotin-avidin interactions in solution. [27]

The activity of enzymes immobilized into porous materials has been extensively investigated. A large number of porous matrices such as polymers, [28] inorganic sol-gels, [29,30] silica [31, 32] and alumina [33] have been used for enzyme immobilization. A number of researchers described the effect of entrapment or attachment of the enzyme to the porous solid support on the overall kinetics of the enzyme. [32, 34, 35] It has been shown that kinetic parameters are affected by several factors. On one hand, the quaternary structure of the enzyme as well as orientation of the tertiary structure is altered by immobilization, which may lead to insufficient exposure of the active site. On the other hand, when immobilization takes place in the porous material other factors such as pore size and morphology, nature of porous material and diffusion of the substrate in and the product out of the pores may contribute to much more complicated kinetic behavior.

The current paper describes the preparation of large and free-standing samples of porous gold from a convenient and not previously used starting material, characterization of the resulting material by scanning electron and atomic force microscopies and its application for immobilization of the enzyme acetylcholine esterase. Efforts are made to estimate the total surface area of the material using solution depletion of a flavin sulfide which forms self-assembled monolayers and is also a strong chromophore, with comparison of the results to classical BET adsorption data. The self-assembled monolayers are studied using cyclic and square-wave voltammetry. The kinetics of the bulk and immobilized enzyme are investigated and compared; and the amount of enzyme adsorbed is estimated.

Materials and Methods

10 Karat (K) white gold (2"×2" piece, 30 GA, 0.25 mm thick) was purchased from Hoover & Strong (Richmond, VA). The stated atomic composition of this commercial alloy, used by jewelers, is 41.8% Au, 5% Ag, 30–35% Cu, 8–9% Zn, and 15–20% Ni. Acetylcholine esterase (AChE) type V-S from *Electrophorus Electricus* as a lyophilized powder, 5,5’-dithiobis-(2-nitrobenzoic acid) (DTNB) and acetylthiocholine were purchased from Sigma-Aldrich (St. Louis, MO). Potassium dihydrogen phosphate and disodium hydrogen phosphate and nitric acid were purchased from Fisher (Pittsburgh, PA). The synthetic flavin derivative (10-(3’-methylthiopropyl)-isoalloxazinyl-7-carboxylic acid) was synthesized in our lab, as previously

reported. [36] Self-assembled monolayers of this compound were previously characterized using electrochemistry, x-ray photoelectron spectroscopy and SEM.

Porous gold was prepared by cutting pieces with a size of 2×2×0.25 mm (geometrical surface area of 0.1 cm^2) and placing them in concentrated nitric acid for different periods of time. A one-day HNO_3 treatment resulted in what will be referred to as surface 1 and a three-day treatment resulted in what will be referred to as surface 2. The sample size was specifically chosen for placing the piece of porous gold in the bottom corner of a standard cuvette, which leaves adequate room for a stir bar. The samples were weighed before and after HNO_3 treatment. After the HNO_3 acid treatment, the samples were rinsed thoroughly with water and were characterized by high-resolution SEM and AFM techniques. UV-visible spectroscopy and electrochemistry studies of the chemisorbed flavin derivative and of the AChE were conducted on these samples. BET analysis was also applied to the samples.

Porous gold surfaces were characterized by SEM and AFM. High-resolution SEM images were acquired on a low-voltage field-emission JSM 6320F SEM (JEOL Inc., Peabody, MA). An electron beam voltage of 5 kV was used to obtain good morphological contrast and high image resolution. Composition of the material obtained by dealloying of 10k gold was determined using the same instrument which has an option of performing energy dispersed spectroscopy (EDS).

A Nanoscope IIIa atomic force microscope (Digital Instruments, Santa Barbara, CA) was used in tapping mode to determine surface roughness. The surface was scanned using NP-20 silicon nitride tips (Veeco Metrology Group, Santa Barbara, CA).

Chemisorption of the synthetic flavin sulfide molecule onto the surface of porous gold was monitored by solution depletion using a UV-visible spectrophotometer (Cary UV 50, Varian, Palo Alto, CA). The porous gold piece was placed in the quartz cuvette containing a 0.2 mM solution of the synthetic flavin in 0.2 M phosphate buffer (pH 6.7). A control experiment was also conducted, in which the absorbance of a solution of the flavin sulfide in the absence of porous gold was monitored as a function of time. The variation of absorbance as a function of time was monitored between 300 and 600 nm for both experiments, with and without porous gold. Stirring of the flavin solution was initiated by a stirrer placed beneath the cuvette (Starna Spinette). The change in absorbance of flavin at 435 nm was used to calculate the remaining concentration of flavin in solution and deduce the number of flavin molecules chemisorbed on the surface of porous gold. For our synthetic derivative, we determined the extinction coefficient for the absorbance at 435 nm to be 3150 M^{-1} cm^{-1}. In their oxidized form, flavins are strong yellow chromophores. The ratio between the number of flavin molecules chemisorbed on the surfaces of porous gold and the number that would be chemisorbed onto a non-porous gold piece of the same size as the sample was calculated and used to estimate the degree of surface area enlargement.

Electrochemical behavior of the flavin derivative chemisorbed on the surface of porous gold was investigated by cyclic voltammetry (CV) and square wave voltammetry (SWV) techniques using a Parstat 2273 (Princeton Applied Research, Oak Ridge, CA). For this purpose, larger samples of porous gold (4×4×0.25 mm) were prepared by the same method described above. Both, surface 1 and surface 2 were thoroughly rinsed with water and methanol and placed in a freshly prepared 0.2 mM methanol solution of flavin sulfide for 24 hours followed by rinsing with methanol and drying. Flavin modified porous gold was then attached to a copper wire with Ag paste (Ted Pella, Inc., Redding, CA) producing flag electrodes for surfaces 1 and 2. Hot glue was used to insulate the connection of porous gold and copper wire as well as to block one side of the flag electrode. As a control, the redox behavior of a self-assembled monolayer

of the flavin derivative chemisorbed on the surface of a standard gold electrode (CH Instruments, Austin, TX) for 24 hours was investigated.

Surface area data for surfaces 1 and 2 were also obtained using a Quantachrome Autosorb-1 automated gas sorption system equipped with Autosorb software, version 1.24 at the Molecular and Nanoscale Analysis Laboratory at Washington University (Saint Louis, MO). Prior to N_2 adsorption all samples were degassed at 100°C for 30 minutes. The surface area of surfaces 1 and 2 was calculated using the multipoint Brunauer-Emmett-Teller (BET) method. To carry out the BET analysis, 10 peices of porous gold (individual size 2×2×0.25 mm) prepared and handled identically were weighted and used in the analysis, thus providing an appropriate mass for the analysis.

In order to immobilize AChE on the surface of the porous gold (surface 1 and surface 2) both surfaces were separately immersed in 0.032 mg/mL solution of AChE (pH 8, 0.1 M phosphate buffer) at 4°C for 24 hours. A similar procedure of 24 hours adsorption was used for the experiments in which the concentration of the enzyme solution was varied. After immobilization of enzyme, both surfaces were rinsed with phosphate buffer in order to remove unbound enzyme. A series of experiments intended to assess the effect of diffusion of the substrate into the pores on the enzyme kinetics were performed. In these experiments two pieces of porous gold (surface 1) were placed into two separate cuvettes and AChE was added at a concentration of 0.032 mg/mL. One of the plates was crushed using a pipette tip immediately after addition of AChE exposing the inner surfaces of the porous gold, followed by 24 h of immobilization. This produced plate A. Another plate was allowed to spend 24 hours in the enzyme solution prior to crushing, producing plate B. Examination of the crushed pieces using an optical microscope and a calibration grid after completion the experiment revealed fragments of size 0.05 mm–1.0 mm, with the almost all of the fragments smaller than 0.3 mm.

Surfaces 1 and 2 and plates A and B have been used to study the kinetics of immobilized AChE and to determine the Michaelis constant (K_m) and maximum velocity of the enzyme catalyzed reaction (V_{max}) as a function of sample treatment and storage time.

The standard Ellman assay [37] was used to study the kinetics of AChE. The principle of the method involves the measurement of the rate of production of thiocholine as acetylthiocholine is hydrolyzed. This is accomplished by reaction of the thiocholine with DTNB to produce the yellow anion of 5-thio-2-nitrobenzoic acid. The rate of the anion color production is determined by measuring the absorbance at 412 nm. For continuous monitoring, a typical run used a porous gold plate with immobilized AChE, which was placed in a plastic cuvette, along with 2910 μL of 0.1 M phosphate buffer (pH 8), 20 μL of 0.01 M DTNB phosphate buffer solution, and 70 μL of 6 mM acetylthiocholine. The plot of absorbance at 412 nm versus time was generated and used to calculate the initial velocity. K_m and V_{max} values were calculated from a Michaelis plot and compared for bulk and immobilized enzyme for the entire range of substrate concentration which varied between 0.02 mM and 0.7 mM. For experiments which involved adsorption of enzyme onto gold from solutions containing different enzyme concentrations the value of the initial velocity for the immobilized enzyme was determined at a fixed substrate concentration of 0.028 mM.

Results and Discussion

Preparation and Characterization of Porous Gold

Dealloying is a common corrosion process during which one or more less-noble elements are removed from an alloy by treatment with concentrated nitric or perchloric acid. [38] Figure 1 shows a top view SEM analysis of porous gold prepared by 24 hour (a) and 72 hour (b) treatment in HNO_3, which corresponds to surfaces 1 and 2 respectively. As it is seen from the figure,

treatment of 10 K gold with HNO_3 results in a highly porous structure. Surface 1 consists of interconnected ligaments, which form uniformly distributed pores that are 50–100 nm in diameter. A longer HNO_3 treatment (surface 2) produces larger ligaments, which are more separated from each other and with larger pores whose diameter is around 200 nm. EDS analysis revealed that these acid treatments removed all elements other than gold to an undetectable level. The formation mechanism of nanoporous structures during dealloying has been described in the literature. [9,39] It has been shown that pores form due to intrinsic dynamic pattern formation during which aggregation of chemically driven noble metal atoms occurs. Figure 2 shows cross sectional SEM analysis of surface 1; these images are similar to the top view images and show formation of a sponge-like structure throughout the sample. Similar images of porous gold prepared by other methods such as sputter coating of a quartz crystal with a thin film of gold and silver followed by dealloying in HNO_3,[40] electrochemical deposition of Au-Zn alloy followed by anodic stripping of Zn,[41] and electrochemical deposition of Au-Ag alloys from the corresponding cyanide solutions followed by dealloying in HNO_3 [11] have been obtained by other authors. It is significant to note that the porous gold structure appears identical on the nanoscale/mesoscale to that reported by other workers, but has emerged from acid treatment of a more complex alloy mixture than typically used binary Au-Ag alloys. Au-Ag alloys form ideal metallic solutions due to their similar structure and almost identical lattice parameters of silver and gold. The alloy used here most likely has a more complex phase diagram and initial microstructure, but has resulted in the same porous gold morphology reported from Au-Ag alloys. Ternary alloys of Au-Ni-Cu, the dominant elements in the alloy used in our experiments, are known to have a two-phase immiscibility gap.[42] The cracks observed on the micron scale by SEM in cross section may be related to the initial microstructure of the alloy, a feature which warrants further investigation, or possibly to volume changes on dealloying. [12]

Figure 3 shows AFM images of surface 1 (a) and surface 2 (b). The generally spherical hills range from 50 to 70 nm in diameter for surface 1 and from 100 to 150 nm in diameter for surface 2. The presence of the spherical hills on the surface can be explained by the fact that every ligament seen in the SEM probably has higher and lower parts, so on the AFM image the upper part appears as a particle-like hill. Three-dimensional topographic images of both surfaces are also presented on Figure 3. The roughness of each surface has been calculated as an arithmetic average of the absolute values of the surface height deviations measured from the mean plane. For surface 1, the roughness was found to be 6.6 nm, whereas for surface 2 it was 30 nm. It is seen that longer treatment of 10 K gold with HNO_3 results in a rougher surface, which is due to the presence of large pores and thicker ligaments. These results are consistent with our SEM data and indicate the value of employing both methods of analysis.

Surface Area Determination and Electrochemical Studies

Chemisorption of flavin sulfide monolayers on the surface of non-porous and 10 K white porous gold (the porous gold resulted from HNO_3 treatment) was investigated by UV-vis spectroscopy and cyclic voltammetry in order to estimate the degree of surface enlargement caused by HNO_3 treatment. This approach was used as an alternate to the BET adsorption isotherm analysis and as a part of the study of the electrochemical behavior of flavin sulfide monolayer in porous gold. Figure 4 shows the structural formula and UV-vis spectra of 0.2 mM flavin sulfide as it chemisorbs onto the surface of porous gold (surfaces 1 and 2) as a function of time. Flavin gives two peaks in the visible region, one at 339 nm, and another at 435 nm. It is seen that as time progresses from zero hours to 24 hours the absorbance decreases for both peaks, which is due to the formation of a self-assembled monolayer of flavin sulfide on the surface of porous gold. An additional spectrum was recorded at 30 hours period, in which a very small increase in the absorbance for both peaks was observed. The increase in absorbance value after 30 hours period is attributed to the saturation of the porous gold sample

and partial desorption of flavin disulfide molecules back into solution. A control experiment where absorbance of flavin was monitored as a function of time in the absence of porous gold material was performed. A 0.2 mM methanol solution of flavin sulfide showed no detectable change in absorbance over 30 hours, indicating that the molecule is stable in solution. Using the change in the absorbance of flavin sulfide at 435 nm, for which $\varepsilon = 3150\ M^{-1}\ cm^{-1}$, one can calculate the number of moles of flavin sulfide depleted from the solution by exposure to the porous gold surface after 24 hours treatment. After 24 hours the number of moles of flavin chemisorbed on the porous gold surface was found to be 3.6×10^{-7} and 2.0×10^{-7} mol for surfaces 1 and 2, respectively. In order to estimate the degree of surface area enlargement one could consider measuring the amount of flavin chemisorbed on the surface of untreated 10 K gold. However, UV-vis spectroscopy can not be used for this purpose due to the undetectable change in absorbance with such a small surface area.

Cyclic voltammetry of a flavin sulfide monolayer chemisorbed on the surface of a standard gold electrode may be used to determine the average area occupied by a flavin sulfide in a SAM on gold. The electroactive part of flavin is the isoalloxazine ring system, which undergoes a $2e^-$, $2H^+$ reversible redox process. The curvature of the ligaments of diameter 50–200 nm is similar to that of the surfaces of large nanoparticles, which are routinely functionalized by thiol and sulfide derivatives. Under the assumption that equivalent SAMs form on porous gold and flat gold, the molecular area per flavin sulfide combined with the change in absorbance can provide an estimate of the surface area and thus the surface enlargement. Previous studies [36] show that the limiting coverage is reached after 6 h of exposure of a flat gold surface to a solution of flavin sulfide and that the resulting SAM exhibits quasi-reversible redox behavior. Figure 5a shows an example of cyclic voltammogram measured for a monolayer of flavin. Integration of the area under the flavin reduction peaks for scanning rates between 0.1 and 0.4 V s^{-1} gives an average surface coverage of 2.9×10^{-10} mol cm^{-2}. The maximum surface occupancy of untreated (flat) surface will be equal to the product of the geometrical area of the untreated piece of white gold (considered as gold, 0.1 cm^2) and the average surface coverage of untreated gold (2.9×10^{-10} mol cm^{-2}), and is equal to 2.9×10^{-11} mol for both surfaces 1 and 2. Our previous SEM and AFM studies showed that the 72 hour HNO_3 treatment produced larger pores and rougher surface and therefore less flavin can be accumulated of surface 2 than on surface 1. The amount of chemisorbed flavin sulfide determined from the UV-vis experiments was found to be 3.6×10^{-7} mol for surface 1 and 2.0×10^{-7} mol for surface 2. For surface 1 this would imply a total surface area of 1240 cm^2; and for surface 2 the data imply a total surface area of 690 cm^2. The ratio between the amounts of flavin adsorbed on treated and untreated gold surfaces suggests that the 24 hour HNO_3 treatment of 10 K white gold gives a 12,400 times surface enlargement, whereas 72 hour treatment enlarges the surface 6900 times. Using the masses of the samples, we obtain 14.2 m^2/g for surface 1 and 8.2 m^2/g for surface 2.

The surface areas of surface 1 and of surface 2 were also determined by using the multipoint Brunauer-Emmett-Teller (BET) method where the adsorption/desorption of nitrogen was used. According to BET analysis, the surface areas of surfaces 1 and 2 were found to be 8.7 m^2/g and 6.5 m^2/g, respectively. Ji and Searson previously determined the surface area of nanoporous gold nanowires by BET analysis.[10] The reported surface area of nanoporous gold, prepared by electrochemical deposition of Ag/Au alloy and followed by HNO_3 dealloying treatment, ranged from 3.7 to 6.9 m^2/g. The porous gold prepared by our method provided higher total surface areas. It is seen that our data obtained by solution depletion studies are in a reasonable agreement with data obtained by BET analysis especially in terms of comparing the two surfaces, which suggests that solution depletion studies can be used as an alternative approach for determination of surface area. A possible explanation for the higher surface area obtained by solution depletion could be the presence of some additional flavin molecules inside the material that are not on the gold surface.

The electrochemical behavior of monolayers of flavin sulfide chemisorbed on the surface of porous gold was also investigated. Figure 5 show typical cyclic voltammograms (5a, 5c and 5e) and square wave voltammograms (5b, 5d, and 5f) for flavin chemisorbed on the surface of a standard gold electrode (5a and 5b), an electrode prepared using surface 1 (5c and 5d) and an electrode prepared using surface 2 (5e and 5f). The cyclic voltammograms were stable over multiple cycles of scanning. As the structure of the electrode changes from non-porous (Figures 5a and 5b) to porous (Figures 5c, 5d, 5e and 5f), the magnitude of the oxidation and reduction currents in the cyclic voltammograms and the magnitude of the oxidation current in the square wave voltammograms increases dramatically due to the significant increase in the electrode surface area. A shift in the oxidation and reduction potentials is also observed for porous electrodes compared to standard gold electrode. For example, the oxidation and reduction potentials for a monolayer of flavin chemisorbed on standard gold electrode are −360 mV and −380 mV respectively giving a ΔE value of 20 mV. These oxidation and reduction potentials are −250 and −520 mV for a porous gold electrode produced from surface 1, and −260 and −520mV for a porous electrode produces from surface 2, giving ΔE values of 270 and 260 mV, respectively. Such a large increase in a ΔE value could be explained by the porous nature of the material and the altered mass transport through the pores of different size, which may be located in the inner or outer parts of the electrode. Therefore, the nanoporous nature of the porous gold electrodes gives a rise to altered electrochemical behavior. The cyclic voltammograms on the porous gold electrode resemble those observed on flat gold at much higher scan rates.[36] Given the involvement of protons in the reduction and oxidation process, limitations on proton diffusion in the porous material might be responsible for slower electron transfer kinetics. The average of the oxidation and reduction potential of flavin on the flat gold electrode is −370 mV, that on surface 1 electrode is −385 mV, and on the surface 2 electrode is −390 mV. Given the sensitivity of the redox behavior of flavin to pH, these small shifts suggest that the pH inside the porous gold is close to that in the bulk solution. The area under the reduction peak in Figure 5c corresponds to a charge of 38,300 μC, and that on Figure 5e corresponds to a charge of 24,000 μC, compared to the charge under the reduction peak in Figure 5a of 2.21 μC. Accounting for the geometrical area of the electrodes (0.03 cm^2 for the standard electrode, and 0.16 cm^2 for the porous gold flag electrodes), results in 56.6 μC cm^{-2} for the standard electrode, and 2.39×10^5 μC cm^{-2} for surface 1 and 1.50×10^5 μC cm^{-2} for surface 2. The ratios of the changes per unit area for the porous gold electrodes to the flat gold electrodes are 4220 and 2650, respectively. Although these ratios are somewhat less than the surface enlargement obtained by solution depletion or BET, it is clear that most of the flavin SAM is electrochemically active and accessible in the porous gold electrode.

Immobilization of Acetylcholine Esterase

One of the potential applications of porous gold material is its use as a solid support for immobilization of biomolecules, which is a critical step to the development of new biosensors and assays. In order to investigate the effect of the new porous gold material on the catalytic properties of enzymes, acetylcholine esterase was chosen due to its high catalytic activity and robustness.[43] Acetylcholine esterase was immobilized on both surfaces of porous gold and the kinetic parameters K_m and V_{max} were determined for the immobilized enzyme. The K_m values were compared between the bulk and immobilized enzyme. The trend in V_{max} and K_m values as a function of storage time was used to assess enzyme stability on the surface. The K_m and V_{max} of the bulk enzyme in a 0.04 μg/mL solution in phosphate buffer pH 8 were found to be 0.08 mM and 5.7×10^{-6} M min^{-1}, respectively. The corresponding k_{cat} value is equal to 665 sec^{-1}, and comparable to those reported by Ramos and Techert, [44] who found that k_{cat} varied with ionic strength.

Figure 6 shows an example of a Michaelis-Menten plot obtained for acetylcholine esterase immobilized on surfaces 1 (figure 6(a)) and 2 (figure 6(b)). Immobilized acetylcholine esterase

obeys Michaelis-Menten kinetics showing saturation at about 2 μM min^{-1} and 1.5 μM min^{-1} for surfaces 1 and 2, respectively. Acetylcholine esterase immobilized on surfaces 1 and 2 (figure 6(a, b)) shows a slight decrease in the velocity of the enzyme catalyzed reaction when the concentration of acetylthiocholine is near 0.8 mM for surface 1 and near 0.4 mM for surface 2. This effect is more pronounced for acetylcholine esterase immobilized on surface 2 (figure 6(b)). The reaction velocity goes back up as the concentration of substrate continues to increase. This could be attributed to the phenomenon known as inhibition by substrate. Inhibition by substrate for acetylcholine esterase has been studied and reported by a number of authors. [45–47] In our case, acetylcholine esterase is immobilized on highly porous material and there are several factors that might trigger inhibition by substrate. One of these factors is the effect of the environment around acetylcholine esterase (porous gold) which may trigger a conformational change in acetylcholine esterase, and result in substrate inhibition. Another factor, which may be responsible for this phenomenon, is some retardation of the deacylation step when binding of a second substrate molecule occurs. This could be presumably due to steric hindrance created by other enzyme molecules immobilized on the highly porous material or by an unfavorable orientation.

Data obtained for K_m and V_{max} values for acetylcholine esterase immobilized on surface 1 and 2 are presented in Table 1. Table 1 shows that upon immobilization of acetylcholine esterase on surfaces 1 and 2 the value of K_m increases as a function of time. During the first day of study, the increase in K_m is similar for both surfaces from 0.08 mM (bulk enzyme) to 0.26 mM (surface 1) and 0.15 mM (surface 2). During the second day of study the value of K_m increases modestly for acetylcholine esterase immobilized on surface 1 (0.74 mM), but changes more dramatically for acetylcholine esterase immobilized on surface 2, where it reaches 2.97 mM. For the sixth day of study the value of K_m reaches 1.14 mM for surface 1 and 2.12 mM for surface 2. The value of V_{max} appears to be more stable for acetylcholine esterase immobilized on surface 2.

The kinetic parameters of enzymes immobilized inside porous materials may be strongly affected even without considering changes in enzyme structure due to interactions with the surface. Surface orientation upon adsorption or immobilization may restrict access to the active site. The surface charge and polarity may alter the substrate concentration near the surface relative to that in the bulk solution. If the substrate concentration is depleted relative to the bulk concentration, an apparent increase in the value of K_m will be observed. When the enzyme is immobilized within a porous material, both external mass transfer to the particle surface and internal mass transfer within the pores must be considered. The substrate concentration may be different form the bulk within the porous material and there may also be a concentration gradient within the material dependent on its geometry. Diffusional restrictions within porous materials often result in higher K_m values. The internal diffusional effects are often described by an effectiveness factor η, which is a ratio of the reaction rate for the immobilized enzyme to that of the free enzyme. [48,49] In the absence of diffusional restrictions η=1, and η increases as diffusional restrictions become more significant. [50] The pore structure and morphology of porous gold might be expected to play a role in the increase of K_m observed for the immobilized enzyme over the K_m measured in bulk solution. The mathematical modeling of enzyme kinetics within porous material is a challenging task.

Pore morphology and size also strongly affects kinetic parameters. Theoretical calculations suggest that maximum stabilization of proteins can be achieved in spherical cages with a diameter of 2–6 times larger than the diameter of the native protein [51] and since the average diameter of hydrated protein is around 10 nm a meso to nanoporous material will provide the maximum stabilization for the protein. The average pore sizes of surfaces 1 and 2 are 50–60 and 150–200 nm, respectively. Surface 1 is a nanoporous material and the behavior of immobilized acetylcholine esterase changes less on this surface, as reflected by the overall

lower K_m value after a 6-day period on surface 1 than on surface 2. A stabilization effect of genetically modified acetylcholine esterase on nanoporous silica beads and meso/nanoporous carbon was also observed by Sotiropoulou and co-workers. [52]

The chemical nature of the porous material may also have an effect on enzyme kinetics. The behavior of proteins on metallic surfaces has been investigated by a number of authors. In particular, Leidbergh and co-workers [53–55] studied the interactions of individual amino acids, L-cysteine, glycine, L-histidine and L-phenylalanine with gold and copper surfaces and they found that interactions between amino acids and metal surface occur via either NH_2 end-groups (Glycine-Au) or through side groups of sulfur-containing amino acids (Cysteine-Au). Thus, when a protein interacts with a porous material it has enough degrees of freedom to take a preferred orientation. Furthermore, the pore size also plays an important role in stabilization of immobilized enzyme. Thus, it can be concluded that the activity of immobilized proteins may be affected by all or a group of the aforementioned parameters.

Experiments in which the porous gold plates were crushed before (plate A) and after (plate B) AChE immobilization have been performed in order to investigate the availability of the enzyme from the inner pores to the substrate as well as the access of the enzyme to the inner pores during adsorption. The K_m values for AChE immobilized on plate A and plate B was found to be 0.32 mM and 0.28 mM, respectively after 24 hours of adsorption. These values are essentially the same as for the intact plates of surface 1, for which K_m= 0.26±0.05 mM after 24 hours of adsorption. Plate A which was crushed prior to enzyme adsorption exhibits a larger V_{max} of 9.0 μM min^{-1} which can be accounted for by the greater area of particle surface available through which enzyme can adsorb into the material. The value of V_{max} found for plate B, crushed after adsorption, is 5.7 μM min^{-1}, which is also larger than that found for the intact plate of surface 1 of 1.85±0.40 μM min^{-1} and indicates that additional enzyme has been made available by exposure of inner surfaces by crushing. If limited diffusion of the substrate into pores was responsible for the observed increase in K_m over the bulk value, then one might expect crushing to have resulted in a smaller observed increase in K_m; however, this was not observed. While diffusion could play a role if the depletion of substrate concentration develops over a very short distance, the observed increase in K_m with storage time would not be consistent with diffusion being a sole factor. The increase in K_m with storage time suggests that the enzyme structure is slowly perturbed by its interaction with the surface over days of storage with the result being a slow decrease in substrate affinity. It is less clear why V_{max} shows signs of increasing as well, although one can speculate that the structural changes are serving to expose more active sites to the substrate.

In order to estimate the amount of the enzyme adsorbed on the surface of porous gold the initial rate of acetylthiocholine hydrolysis at 0.028 mM was monitored as a function of enzyme concentration used for immobilization of acetylcholine esterase on the surface 2. The substrate concentration chosen is well below the value of K_m in the range where the initial rate (v_o) is linearly proportional to substrate concentration and where the rate at fixed substrate concentration should also be linearly proportional to enzyme concentration. In these experiments the supernatant liquid above the surface was removed and v_o was determined separately. The value of v_o for the enzyme on the surface was also determined separately. Table 2 presents the variations of the initial rates determined in the supernatant liquid and on the porous gold surface at constant concentration of acetylthiocholine for different concentrations of acetylcholine esterase. Each entry represents the average of results for two independently prepared plates. At low enzyme concentration, the initial rate of acetylthiocholine hydrolysis is significantly higher for adsorbed enzyme than for the enzyme which remains in the solution. However, as initial concentration of the enzyme increases the initial rate values become closer to each other and reach an almost identical value when 0.034 mg/mL of enzyme was used for immobilization. As it is also seen from the table, variation of enzyme concentration from 0.011

mg/mL to 0.091 mg/mL has less appreciable effect on the initial rate value which varies between 2.2–2.6 μM min^{-1}. Comparison of the initial rates determined for supernatant liquid and porous gold plate can be used to study partitioning of the enzyme between the supernatant liquid and the porous gold plate and can also be used to determine the amounts of adsorbed enzyme assuming that the catalytic constant (k_{cat}) and K_m for bulk enzyme in the solution from which enzyme adsorption occurs and the enzyme contained in the supernatant liquid have the same values. Initial rates of acetylthiocholine hydrolysis by acetylcholine esterase before and after its adsorption on the porous gold surface can be written as follows:

$$v_{o,\text{bulk}}=(k_{\text{cat,bulk}}/K_{m,\text{bulk}})[E]_o[S] \quad (1)$$

$$v_{o,SN}=(k_{\text{cat},SN}/K_{m,SN})[E]_{SN}[S] \quad (2)$$

where $v_{o,bulk}$ is the initial rate in the bulk enzyme solution prior to adsorption onto porous gold, $v_{o,SN}$ is the initial rate in the supernatant enzyme solution remaining after enzyme adsorption, $[E]_o$ is the initial enzyme concentration, $[E]_{SN}$ is the enzyme concentration in the supernatant, and [*S*] is the concentration of substrate added to determine the initial rates. In our experiments, [*S*]=0.028 mM was used to determine $v_{o,bulk}$ and $v_{o,SN}$. Assuming that $k_{cat\ ,bulk} = k_{cat\ ,SN}$ and $K_{m,\ bulk} = K_{m,SN}$ we can divide equation (2) by equation (1) to obtain

$$\frac{v_{o,SN}}{v_{o,\text{bulk}}}=\frac{[E]_{SN}}{[E]_o} \quad (3)$$

Using the ratio of initial rates and the known value of $[E]_o$, the value of $[E]_{SN}$ can be determined. The amount of adsorbed enzyme can be determined using

$$[E]_{ads}=[E]_o-[E]_{SN} \quad (4)$$

and then the amount of enzyme adsorbed can be calculated from $[E]_{ads} \times V_{bulk}$, where V_{bulk} is the volume of the solution from which enzyme adsorption occurred, in this case V_{bulk} = 1 mL. The calculated amounts enzyme are presented in table 2. The calculated amounts of adsorbed enzyme are seen to increase with enzyme concentration with the exception of the highest concentration; it is possible that some blockage of the pores on the surface of the material may have occurred.

The value of k_{cat} was calculated on the basis of the amount of adsorbed enzyme and V_{max} value determined for surface 2 and was found to be 1.7 sec^{-1}. This estimate of k_{cat} for the immobilized enzyme assumes that all of the immobilized enzyme is accessible and functioning at saturation. Given the increase in V_{max} observed for crushing after adsorption (plate B), this is unlikely and the real value of k_{cat} for the immobilized enzyme is very likely to be higher by at least a factor of 3x this estimate. This value is much smaller compared to bulk enzyme (665 sec^{-1}), which means that the amount of the active sites which catalyze hydrolysis of acetylthiocholine is significantly lower. However, other kinetic parameters (K_m and V_{max}) show even with reduced number of active sites, AChE immobilized on the surface of porous gold is fully functional and relatively stable.

The quantities of the enzyme adsorbed are in the sub-monolayer regime. The radius of gyration of type V-S acetylcholine esterase from *Electrophorus Electricus* was determined by small angle X-ray scattering to be 48.88 Å including a 3 Å wide hydration shell. [44] Assuming a footprint per enzyme molecule on the gold surface of 95 nm^2, then for surface 2 one would obtain a capacity of 7.3×10^{14} enzyme molecules in a ideally arranged monolayer. Acetylcholine esterase has a mass of 280 kDa. Thus, the number of enzyme molecules adsorbed, based on the results in table 2, range from a low of 6.2×10^{11} to a maximum of 2.8×10^{13}. The coverage of enzyme on the surface obtained by physical adsorption thus falls in a sub-monolayer regime. Increasing the enzyme coverage would likely require either much

longer adsorption times or the pursuit of covalent immobilization strategies. Covalent immobilization, such as to SAM-modified porous gold, might result in more stable kinetic parameters and better behavior during storage.

Conclusions

In this paper, we reported the preparation, characterization and application of porous gold material. A simple approach to the fabrication of large, free-standing and high surface area porous gold material by dealloying commercially available 10K white gold with concentrated nitric acid is demonstrated. We have shown that the pore structure and morphology of the final porous gold sample can be altered by variation of the dealloying time: a 24 hour HNO_3 treatment produces a porous gold with 12,400-fold surface enlargement while a 72 hour HNO_3 treatment yields a porous gold with 6900-fold surface enlargement. The nano and mesoporous gold surfaces were used as a solid support for the enzyme acetylcholine esterase, which demonstrates the potential applicability of this material for biosensor development. The dependence of activity of immobilized enzyme on the size and structure of pores in porous gold was studied. Our experimental data shows that nanoporous gold, with average pore sizes about 50 nm in diameter, is more suitable for immobilization of acetylcholine esterase.

Acknowledgment

The authors are grateful to Professor Cynthia Dupureur (University of Missouri – St. Louis, Department of Chemistry and Biochemistry) for discussions on some aspects of enzyme kinetics. This project is financially supported by the National Institute of Health (NIH grant 5R21GMO72693-02).

References

1. West JL, Hatas NJ. Ann. Rev. Biomed. Eng 2003;5:285–296. [PubMed: 14527314]
2. Ding Y, Chen MW, Erlebacher J. J. Amer. Chem. Soc 2004;126:6876–6877. [PubMed: 15174851]
3. Shukla S, Priscilla A, Banerjee M, Bhonde R, Ghatak J, Satyam PV, Sastry M. Chem. Mater 2005;17:5000–5005.
4. Gregory S, Torsten R, Burkhard R. J. Electroanal. Chem 2002;526:125–133.
5. Csathy GA, Tulimieri D, Yoon J, Chan MHW. Phys. Rev. Lett 1998;80:4482–4485.
6. Bonroy K, Friedt J-M, Frederix F, Laureyn W, Langerock S, Campitelli A, Sara M, Borghs G, Goddeeris B, Declerck P. Anal. Chem 2004;76:4299–4306. [PubMed: 15283564]
7. Wang X-Y, Zhong H, Lv Y, Chen H-Y. Chem. Lett 2003;32:1054–1055.
8. Noort D, Rani R, Mandenius C-F. Microchim. Acta 2001;136:49–53.
9. Erlebacher J, Aziz M, Karma A, Dimitrov N, Sieradzki K. Nature 2001;410:450–453. [PubMed: 11260708]
10. Ji C, Searson PC. J. Phys. Chem. B 2003;107:4494–4499.
11. Dursun A, Pugh DV, Corcoran SG. J. Electrochem. Soc 2005;152:B65–B72.
12. Parida S, Kramer D, Volkert CA, Erlebacher J, Weissmüller J. Phys. Rev. Lett 2006;97:035504-1–035504-4. [PubMed: 16907511]
13. Wagner K, Brankovic SR, Dimitrov N, Sieradzki K. J. Electrochem. Soc 1997;144:3545–3555.
14. Attard GS, Bartlett PN, Coleman NRB, Elliot JM, Owen J, Wang JH. Science 1997;278:838–840.
15. Jurczakowski R, Hitz C, Lasia A. J. Electroanal. Chem 2004;572:355–366.
16. Hoogvliet JC, Dijksma M, Kamp B, Bennekom WP. Anal. Chem 2000;72:2016–2021. [PubMed: 10815959]
17. Walsh D, Arcelli L, Ikoma T, Tanaka J, Mann S. Nature Mater 2003;2:386–390. [PubMed: 12764358]
18. Sieradzki K, Dimitrov N, Movrin D, McCall C, Vasiljevic N, Erlebacher J. J. Electrochem. Soc 2002;149:B370–B377.
19. Senior NA, Newman RC. Nanotech 2006;17:2311–2316.

20. Haung J-F, Sun I-W. Adv. Funct. Mater 2005;15:989–994.
21. Duan C, Meyerhoff M. Mikrochim. Acta 1995;117:195–206.
22. Duan C, Meyerhoff M. Anal.Chem 1994;66:1369–1377. [PubMed: 8017631]
23. Ducey M, Meyerhoff M. Electroanalysis 1998;10:157–162.
24. Jurica L', Manova A, Dzurov J, Beihrohr E. Fresenius J. Ana. Chem 2000;366:260–266.
25. Cai W-Y, Xu Q, Zhao X-N, Zhu J-J, Chen H-Y. Chem. Mater 2006;18:279–284.
26. Tipple CA, Lavric NV, Culha M, Datskos P, Sepaniak MJ. Anal. Chem 2002;74:3118–3126. [PubMed: 12141672]
27. Lavric NV, Tipple CA, Sepaniak MJ, Datskos PG. Biomed. Microdev 2001;2:35–44.
28. Berlin P, Klemm D, Jung A, Liebegott H, Rieseler R, Tiller. J. Cellulose 2003;10:343–367.
29. Park C, Clark DS. Biotechnol. Bioeng 2002;78:229–235. [PubMed: 11870613]
30. Lei C, Shin Y, Liu J, Ackerman EJ. J. Am. Chem. Soc 2002;124:11242–11243. [PubMed: 12236718]
31. DeLouise L, Miller B. Anal.Chem 2005;77:1950–1956. [PubMed: 15801723]
32. Drott J, Rosengren L, Lindstrom K, Laurell T. Thin Solid Films 1998;330:161–166.
33. Vasudevan PT, Thakur DS. Appl. Biochem. Biotechnol 1994;49:173–189. [PubMed: 7847895]
34. Blaedel WJ, Kissel TR, Boguslaski RC. Anal.Chem 1972;44:2030–2037. [PubMed: 4657296]
35. Kerby MB, Legge RS, Tripathi A. Anal. Chem 2006;78:8273–8280. [PubMed: 17165816]
36. Stine KJ, Andrauskas DM, Khan AR, Forgo P, D'Souza VT, Liu J, Friedman RM. J. Electroanal. Chem 1999;472:147–156.
37. Ellman G, Courtney K, Andres V, Featherstone R. Biochem. Pharmacol 1961;7:88–95. [PubMed: 13726518]
38. Erlebacher J, Sieradzki K. Scripta Materialia 2003;49:991–996.
39. Li R, Sieradzki K. Phys. Rev. Lett 1992;68:1168–1171. [PubMed: 10046097]
40. Hieda M, Garcia R, Dixon M, Daniel T, Allara D, Chan MHW. App. Phys. Lett 2004;84:628–630.
41. Huang J-F, Sun I-W. Adv. Func. Mater 2005;15:989–994.
42. Grimwade M. Gold Tech 2000;30:8–15.
43. Rosenberry TL. Adv. Enzymol. Related Areas of Molecular Biology 1975;43:103–218.
44. Ramos A, Techert S. Biophys. J 2005;89:1990–2003. [PubMed: 15994894]
45. Gao J-R, Rao JV, Widle G, Zhu KY. Arch. Insect. Biochem. Physiol 1998;39:118–125. [PubMed: 9880902]
46. Krupka RM. Biochem 1963;2:76–82. [PubMed: 13927118]
47. Radic Z, Reiner E, Taylor P. Mol. Pharmacol 1991;39:98–104. [PubMed: 1987454]
48. Gomez JL, Bodalo A, Gomez E, Bastida J, Maximo MF. Chem. Eng. Sci 2003;58:4287–4290.
49. Ueyama K, Furusaki S. Chem. Eng. Commun 1985;36:299–316.
50. Bailey, JE.; Ollis, DF. Biochemical Engineering Fundamentals. New York: McGraw-Hill; 1986.
51. Wie Y, Xu J, Feng Q, Dong H, Lin M. Mater. Lett 2000;44:6–11.
52. Sotiropoulou S, Vamvakaki V, Chaniotakis N. Biosens. Bioelectron 2005;20:1674–1679. [PubMed: 15626627]
53. Leidbergh B, Lundstrom I, Wu CR, Salanek WR. J. Coll. Interface Sci 1985;108:123–131.
54. Ihs A, Leidbergh B. J. Coll. Interface Sci 1991;144:282–292.
55. Leidbergh B, Carlsson C, Lundstrom I. J. Coll. Interface Sci 1987;120:64–75.

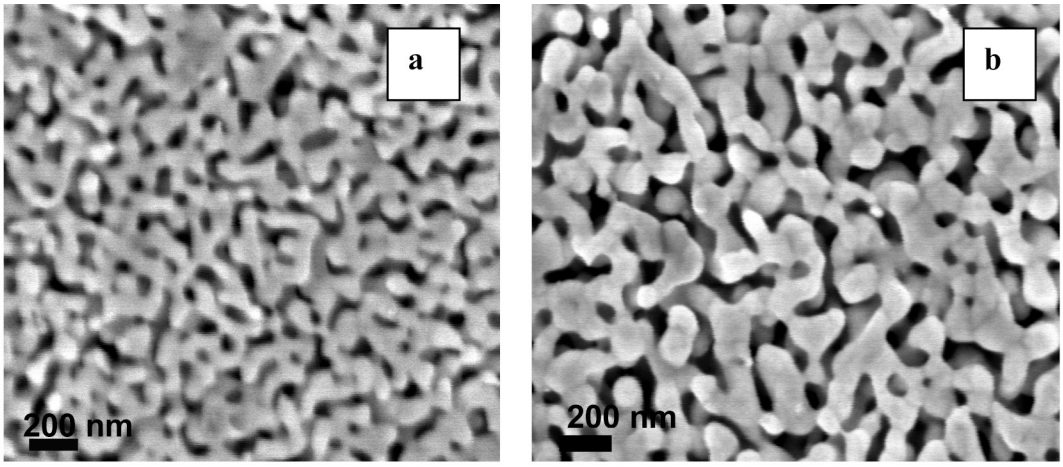

Figure 1.
SEM of porous gold prepared by 24 hours (a) and 72 hours (b) HNO_3 treatments. Magnification is 100,000x.

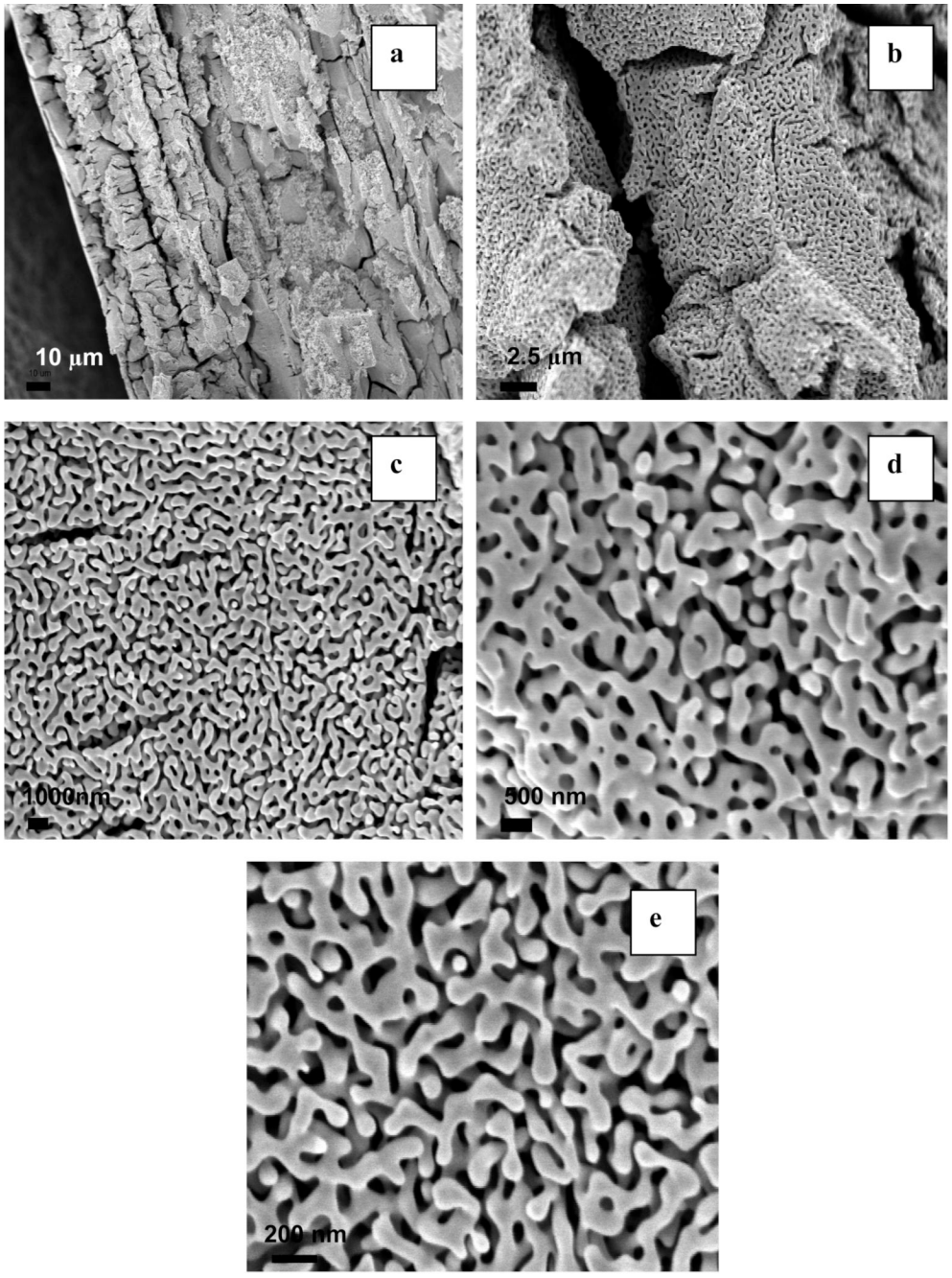

Figure 2.
Cross-sectional SEM images of surface 1 at different magnifications: (a) 1,000 (b) 10, 000x, (c) 20,000x, (d) 50,000x and (e) 100,000x times.

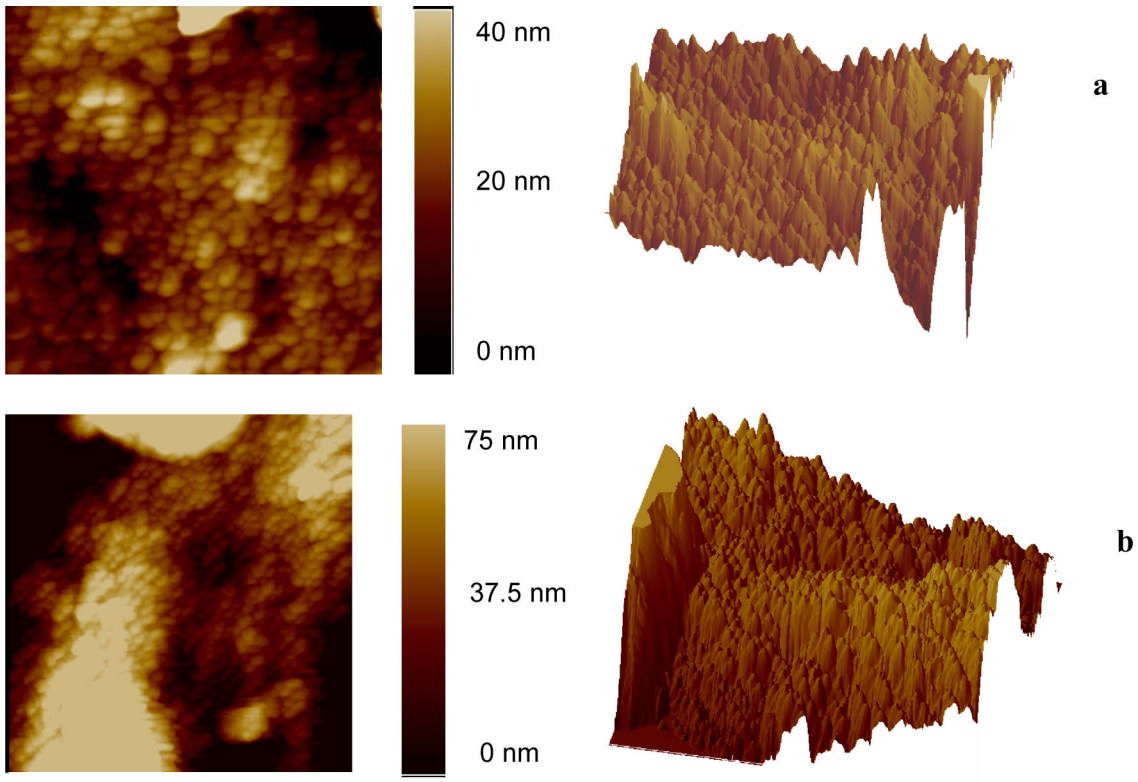

Figure 3.
Typical AFM images of porous gold. (a) surface 1, scan size 1 × 1 μm, (b) surface 2, scan size 3 × 3 μm

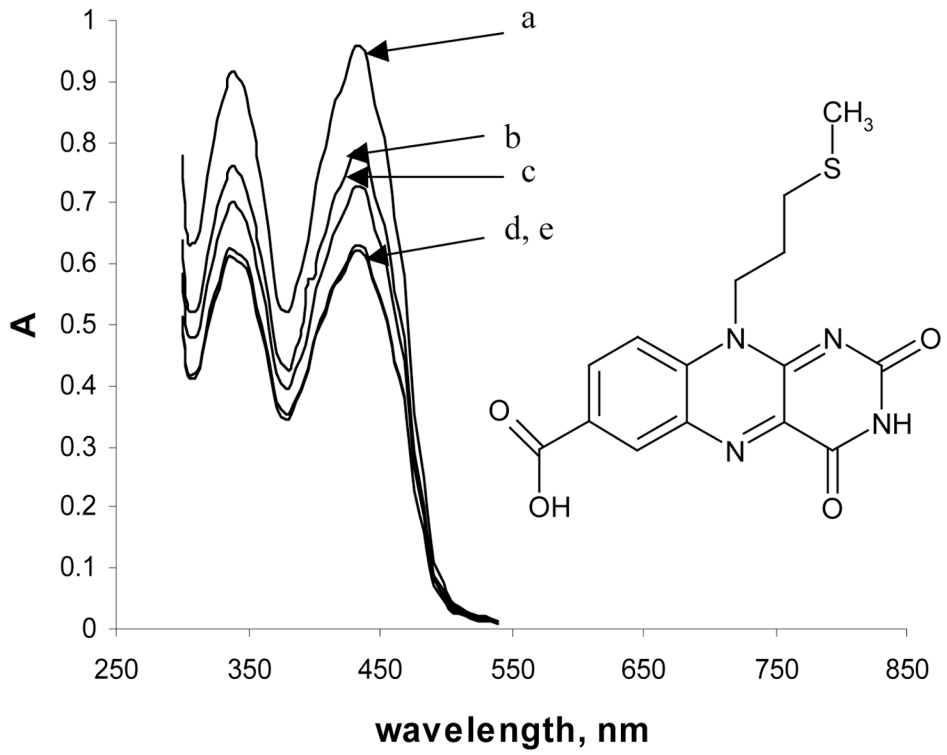

Figure 4.
Spectrum of a 0.2 mM solution of flavin in phosphate buffer (pH 7) as it chemisorbs onto the surface of porous gold (surface 1, 2×2.1×0.25 mm) at different times: (a) initial spectrum, (b) after 3 hours, (c) after 6 hours, (d) after 24 hours, (e) after 30 hours.

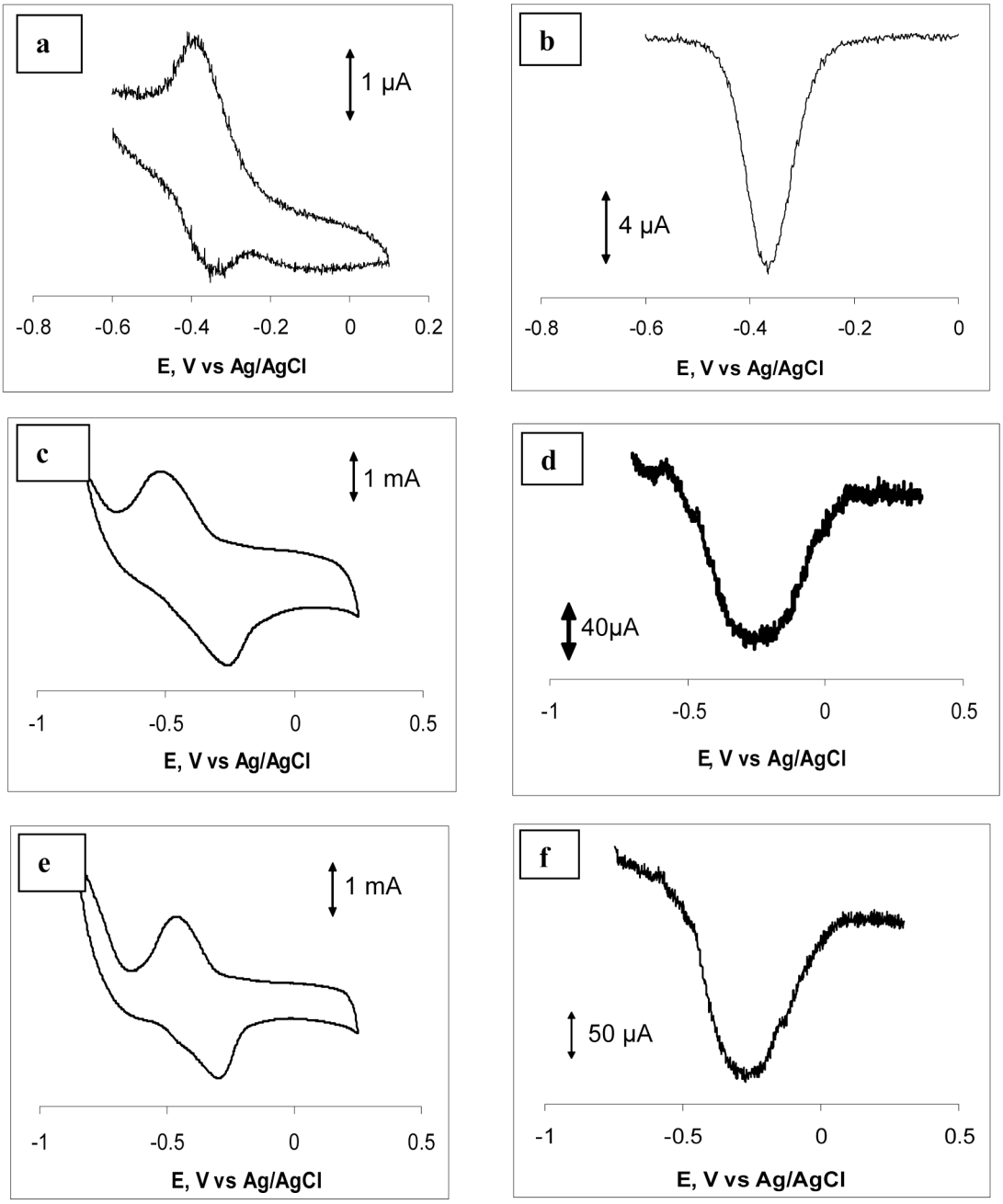

Figure 5.

Cyclic voltammetric (a, c, e) and square wave voltammetric (b, d, f) responses of flavin modified standard gold electrode (a, b), porous gold flag electrode prepared of surface 1 (c, d) and porous gold flag electrode prepared of surface 2 (e, f) in 0.015 M phosphate buffer pH 6.7. Scanning performed in positive direction at a rate of 100 mV/sec.

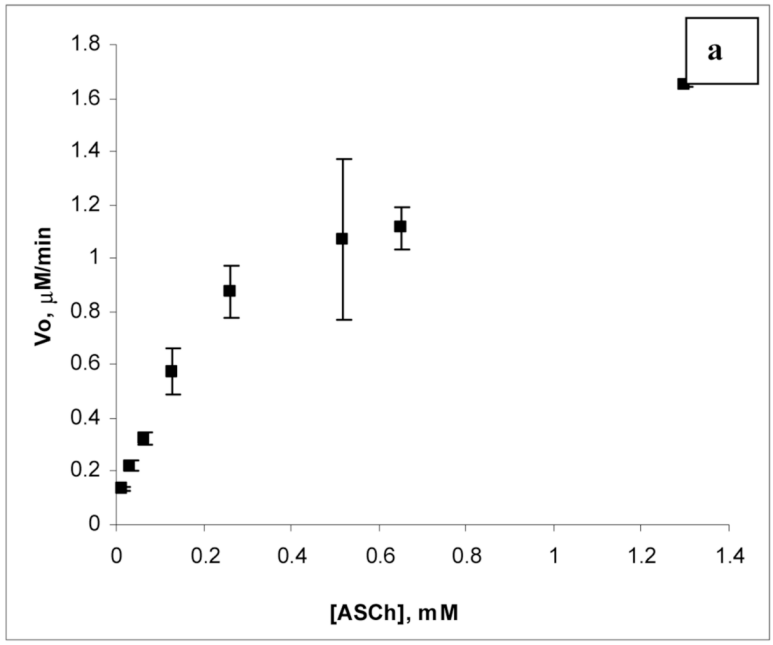

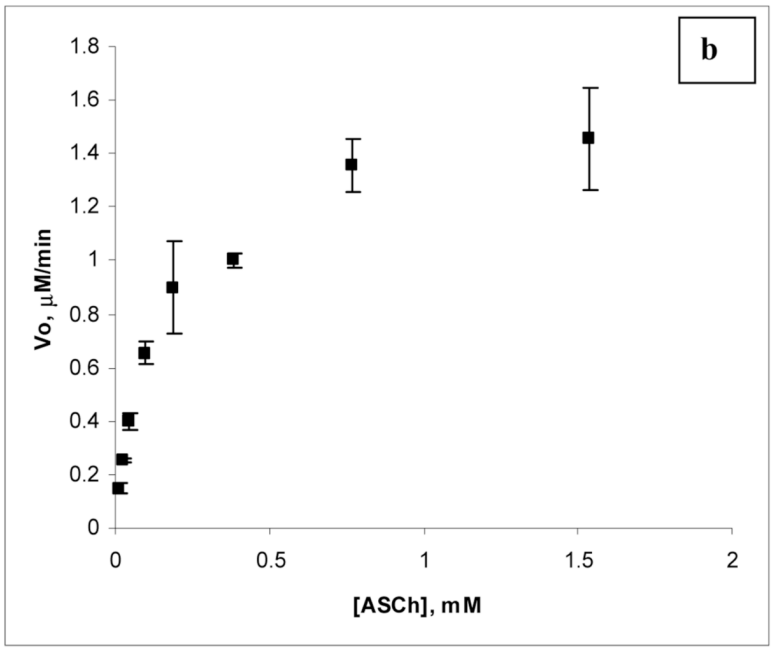

Figure 6.
An example of a Michaelis-Menten plot for acetylcholine esterase immobilized on surface 1 (a) and surface 2 (b); both plots correspond to the first day after immobilization.

Table 1

Variation of kinetic parameters for acetylcholine esterase immobilized on porous gold*.

	Surface 1		Surface 2	
Days	K_m, mM	V_{max}, μM/ min	K_m, mM	V_{max}, μM/ min
1	0.26 (0.05)	1.85(0.40)	0.15 (0.04)	1.56 (0.17)
2	0.74 (0.1)	3.0 (0.43)	2.97 (0.9)	1.18 (0.15)
3	1.82 (0.3)	4.23 (0.45)	1.41 (0.56)	3.73 (0.63)
6	1.14 (0.3)	2.03 (0.46)	2.12 (0.33)	2.75 (0.3)

* All experiments were repeated in triplicate. Standard deviations are given in the parenthesis.

Table 2

Comparison of the initial rates (V_o) of acetylthiocholine hydrolysis at 0.028 mM by acetylcholine esterase in the supernatant liquid (SNT) and on the surface of porous gold plate.

Enzyme concentration mg/ml	V_o (μM/min) at 0.028 mM acetylthiocholine		Amount of the enzyme, mg	
	SNT	Plate	$[E]_{SN}$	$[E]_{ads}$
1.2×10^{-3}	0.11	0.46	0.91×10^{-3}	0.29×10^{-3}
2.9×10^{-3}	0.18	0.44	2.54×10^{-3}	0.36×10^{-3}
0.011	0.8	2.52	9.3×10^{-3}	1.7×10^{-3}
0.034	1.82	2.23	21×10^{-3}	13×10^{-3}
0.091	6.07	2.64	88×10^{-3}	3×10^{-3}